Available online at www.sciencedirect.com

SciVerse ScienceDirect

Ceramics International 39 (2013) 233–238

CERAMICS INTERNATIONAL

www.elsevier.com/locate/ceramint

Optical and mechanical properties of amorphous bulk and eutectic ceramics in the HfO_2–Al_2O_3–Y_2O_3 system

Li-Li Wang[a], Lin Mei[b,c], Guang-Hua Liu[b], Gang He[b,c], Jiang-Tao Li[b,*], Li-Hua Xu[a]

[a]Department of Materials Science and Engineering, University of Science and Technology, Beijing 100083, China
[b]Technical Institute of Physics and Chemistry, Chinese Academy of Sciences, Beijing 100190, China
[c]Graduate School of the Chinese Academy of Sciences, Beijing 100039, China

Received 29 May 2012; received in revised form 3 June 2012; accepted 4 June 2012
Available online 13 June 2012

Abstract

Bulk glasses containing HfO_2 nano-crystallites of 20–50 nm were prepared by hot-pressing of HfO_2–Al_2O_3–Y_2O_3 glass microspheres at 915 °C for 10 min. By annealing at temperatures below 1200 °C, the bulk glasses were converted into transparent glass-ceramics with HfO_2 nano-crystallites of 100–200 nm, which showed the maximum transmittance of ~70% in the infrared region. An increase of annealing temperature (> 1300 °C) resulted in opaque YAG/HfO_2/Al_2O_3 eutectic ceramics. The eutectic ceramics contained fine Al_2O_3 crystallites and showed a high hardness of 19.8 GPa. The fracture toughness of the eutectic ceramics increased with increasing annealing temperature, and reached the maximum of 4.0 MPa $m^{1/2}$.

Keywords: Amorphous sintering; Transparency; HfO_2–Al_2O_3–Y_2O_3; Eutectic ceramics

1. Introduction

Considerable efforts have been made to develop eutectic ceramics in the ZrO_2–Al_2O_3–Y_2O_3/$Y_3Al_5O_{12}$ (YAG) system by melt quenching [1–3], rapid solidification [4] and directional solidification [5,6] for their excellent high-temperature chemical innerness and mechanical properties. HfO_2 and ZrO_2 are known for their similar structure, properties and applications. As against ZrO_2, HfO_2 possesses higher chemical stability and lower thermal expansion coefficient. So the HfO_2–Al_2O_3–Y_2O_3 (HAY) system is likely to be promising as structure and/or functional materials in aggressive environments.

However, experiment information about the HfO_2-involved eutectic ceramics is absent in literature except the research of Araki et al. on the HfO_2–Al_2O_3–Gd_2O_3 eutectic ceramics [7–9] and the reports of Lakiza et al. on the HfO_2–Al_2O_3–Y_2O_3 phase diagram [10–13]. Araki et al. fabricated the amorphous phase with the HfO_2–Al_2O_3–Gd_2O_3 eutectic composition by the arc-image furnace and then obtained transparent nano-composite ceramics by post-annealing. However, the amorphous bulk "ceramics" were limited in diameter size (about 5–7 mm) because both, the very high melting temperature and the high cooling rate were necessary to obtain a large-size glass in this system [7–9]. On the other hand, the network modifier oxide Gd_2O_3 resulted in a meta-stable $GdAlO_3$ phase in eutectic ceramics, which might influence the high-temperature stability. Hence, developing bulk glasses or ceramics with high-temperature stable phases in the HfO_2-involved system is interesting for a wide range of applications in structural materials.

This paper reports the fabrication of bulk HfO_2–Al_2O_3–Y_2O_3 glasses by amorphous sintering [14–17]. By annealing the bulk glasses, transparent glass-ceramics or opaque eutectic ceramics have been prepared. The effect of annealing temperature on the phase assemblage, microstructure, optical and mechanical properties of as-prepared samples are discussed.

2. Experimental procedures

High purity HfO_2 (99.99%, China Minmetals (Beijing) Research Institute), Al_2O_3 (99.99%, Dalian Luming

*Corresponding author.
E-mail address: ljt0012@vip.sina.com (J.-T. Li).

0272-8842/$36.00
http://dx.doi.org/10.1016/j.ceramint.2012.06.015

Nanometer Material Co., Ltd.) and Y_2O_3 (99.99%, China Minmetals (Beijing) Research Institute) powders were used as raw materials. The three powder mixtures were ball-milled in ethanol for 24 h with the molar composition of $14HfO_2$–$63Al_2O_3$–$23Y_2O_3$. According to the HfO_2–Al_2O_3–Y_2O_3 phase diagram [10–13], the ternary composition studied in this work locates in the quasiternary eutectic section of $YAG/Al_2O_3/HfO_2$. The spry-dried powder mixtures were water-quenched into glass microspheres of about 20–100 μm by C_2H_2/O_2 flame melting [18,19]. To fabricate bulk glasses, the batches of glass microspheres were loaded into Φ20 and/or 40 mm graphite die and then hot-pressed at prescribed temperatures for 10 min under the pressure of 60 MPa. All of the sintering temperatures (T_s) are within the kinetic window to avoid devitrification [20], i.e. $T_g < T_s < T_{onset}$, where T_g is the glass transition temperature and T_{onset} is the onset crystallization temperature. The combination of flame-quenching and amorphous sintering makes the size of refractory oxides glass increase to a centimeter or even larger one if the sintering equipment permits. We obtained the transparent glass-ceramics containing nano-crystallites by post-annealing the bulk glasses at lower temperatures (< 1200 °C) and eutectic ceramics at a series of higher temperatures ranging from 1300 to 1500 °C.

The glass transition temperature (T_g) and onset crystallization temperature (T_{onset}) of the glass microspheres were determined by a differential thermal analysis (DTA, NETZSCH STA 449C, Germany). XRD analysis of the as-sintered glasses and ceramics were performed by X-ray diffraction (XRD, D8 Focus, Bruker, Germany) using Cu Kα radiation. The flied emission scanning electron microscopy (FESEM, Hitachi S-4800, Japan) and transmission electron microscopy (TEM, JEOL JEM 2100F, Japan) were used to investigate the microstructures of glasses and glass-ceramics. The in-line transmittance spectra were obtained using an UV–VIS–NIR spectrophotometer (Cary5000, Varian, America) for 175–2000 nm and a Fourier transform infrared spectra (FTIR; Excalibur 3100, Varian, America) for the range from 2000 nm to 25 μm. All the samples were polished down to 1 mm thick.

The densities of samples were measured by the Archimedes method, and the theoretical density of HAY glass can be calculated to be 4.29 g/cm^3 by an empirical equation [21]:

$$\rho_{th} = 0.53\frac{\Sigma(M_i x_i)}{\Sigma(M_i x_i)} \quad (1)$$

where M_i is the molar weight (kg/mol), x_i is the molar fraction (mol%), and V_i is the packing density parameter (m^3/mol) for an oxide M_XO_Y. Vickers hardness (H_v) was measured under loads of 300 g using a microhardness machine (HXD-1000TM, Shanghai, China). Fracture toughness (K_{IC}) was calculated from Eq. (2) [22]:

$$K_{IC} = 0.035\left(\frac{H_v}{E}\right)^{-2/5}\left(\frac{c}{a}-1\right)^{-1/2}H_v\sqrt{a}\Phi^{-3/5} \quad (2)$$

where E is the Young modulus of the material, a is the half-length of the diagonal, c is the crack length measured from the middle of the indent to the tip of the crack and Φ is the constraint factor, usually assumed as 2.7.

3. Results and discussion

3.1. Preparation of HAY bulk glasses by hot-pressing

To realize full densification by plastic flow (creep) before devitrification, the glass microspheres were hot pressed at a series of temperatures below T_{x1} (923 °C, determined by DTA analysis shown in Fig. 1), i.e. 905, 910, 915 and 920 °C. The density of hot-pressed glass samples increased by increasing hot-pressing temperature, as shown in Fig. 2, which demonstrates that a higher temperature is favorable for deformation by plastic flow. As a result, the transmittances of bulk glasses were improved when the sintering temperature increased from 905 to 915 °C. The fact that all of the experimental densities were larger than the calculated value (4.29 g/cm^3) implies a more impacted microstructure in the glass matrix. X-ray spectra in Fig. 3 indicate that after hot pressing HfO_2 crystallites precipitated in the glass matrix and further grew up with the increasing hot-pressing temperature. This contributes to the increasing glass densities and the decreasing transmittances for the glass sintered at 920 °C.

The lower density of the sample sintered at 905 °C is further confirmed by the existence of many pores at the boundaries of the glass microspheres, as shown in Fig. 4(a). As a result, its transmittance is below 60% even in the infrared region (Fig. 2(a)). When the sintering temperature increases to 915 °C, plastic deformation proceeds and the interparticle pores eventually disappear (Fig. 4(b)). The top transmittance reaches ~70% at the infrared range of 4–5 μm but the particle boundary still

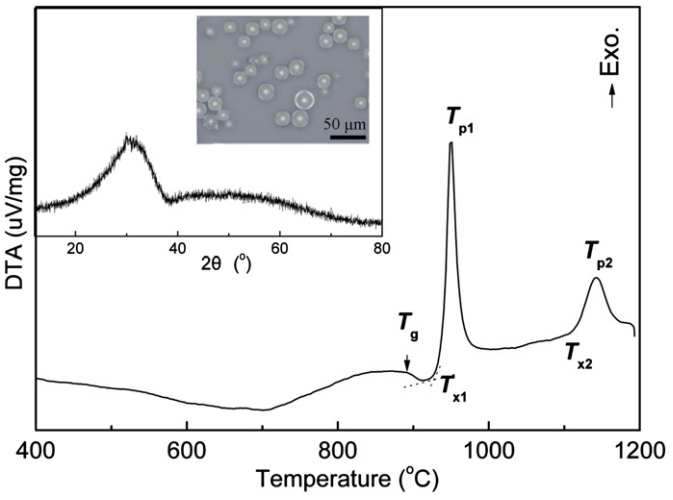

Fig. 1. DTA trace of HAY glass microspheres at the heating rate of 10 °C/min. The insets show XRD pattern of HAY glass microsphere and its optical micrograph.

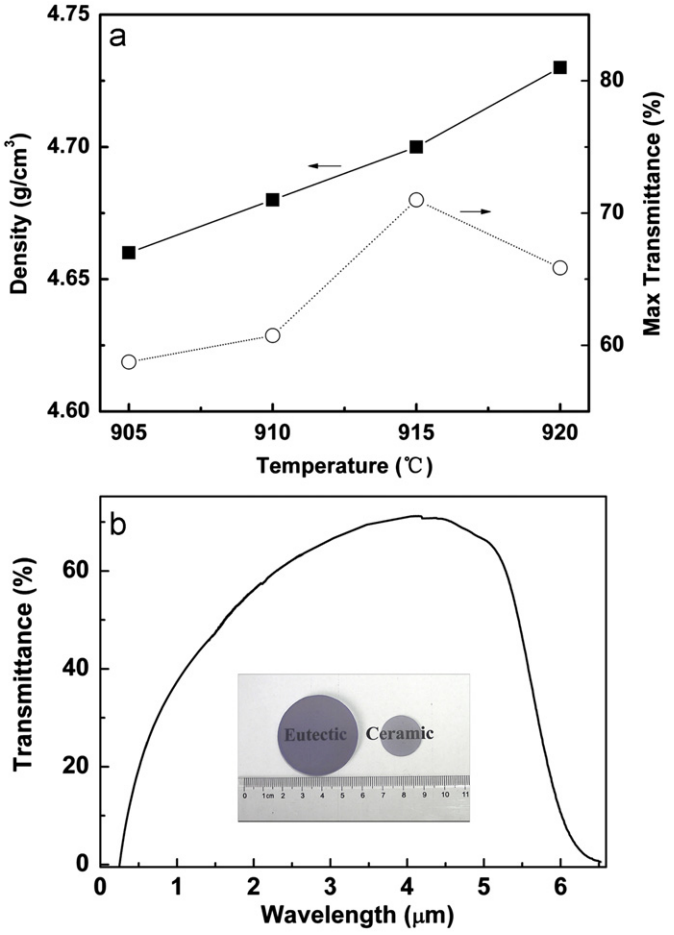

Fig. 2. (a) Dependence of the density and the transmittance of as-prepared glasses on the sintering temperature; (b) transmittance curve of HAY glass hot-pressed at 915 °C, and the inset shows photographs of Nd-doped HAY glasses with a Nd^{3+} concentration of 0.6 wt% (left) and 0.3 wt% (right), respectively. The thickness of the samples is 1 mm.

can be observed, which contributes to the poor transparence in the visible region (Fig. 2(b)).

3.2. Production of glass-ceramics and eutectic ceramics by annealing HAY glasses

According to DTA results (Fig. 1), there are two crystallization peaks during the heat treatment, i.e. at $T_{p1}=949$ °C and $T_{p2}=1142$ °C, respectively. This indicates that the crystallization occurs by two steps during the heat treatment, similar with the crystallization path of HfO_2–Al_2O_3–Gd_2O_3 eutectic composition. To confirm the crystallization of HfO_2–Al_2O_3–Y_2O_3 eutectic composition, the samples annealed at the temperatures ranging from 1000 to 1500 °C were investigated by XRD. The results (Fig. 5) indicate that the first crystallization peak (at 949 °C) corresponds to the crystallization of HfO_2 and the second one (at 1142 °C) corresponds to the crystallization of YAG. After annealing at temperatures above 1300 °C, Al_2O_3 was also observed. It means that crystallization of HfO_2, YAG and Al_2O_3 can be controlled by appropriable

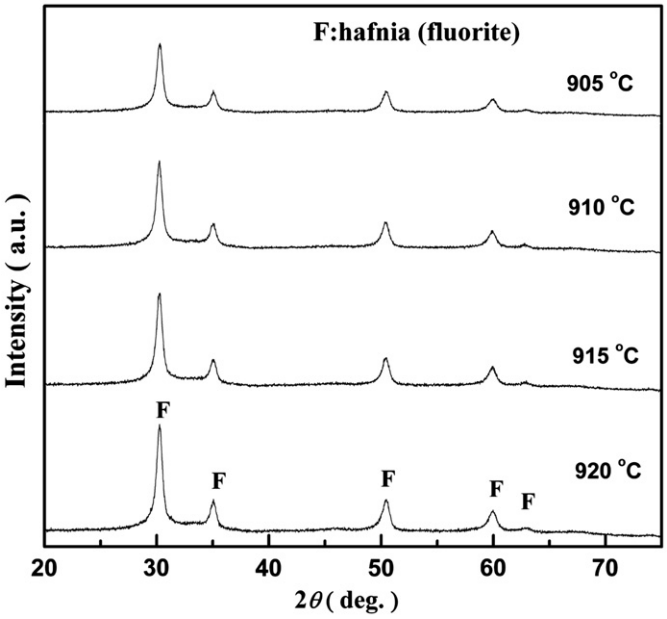

Fig. 3. XRD patterns of HAY bulk glasses hot-pressed at different temperatures.

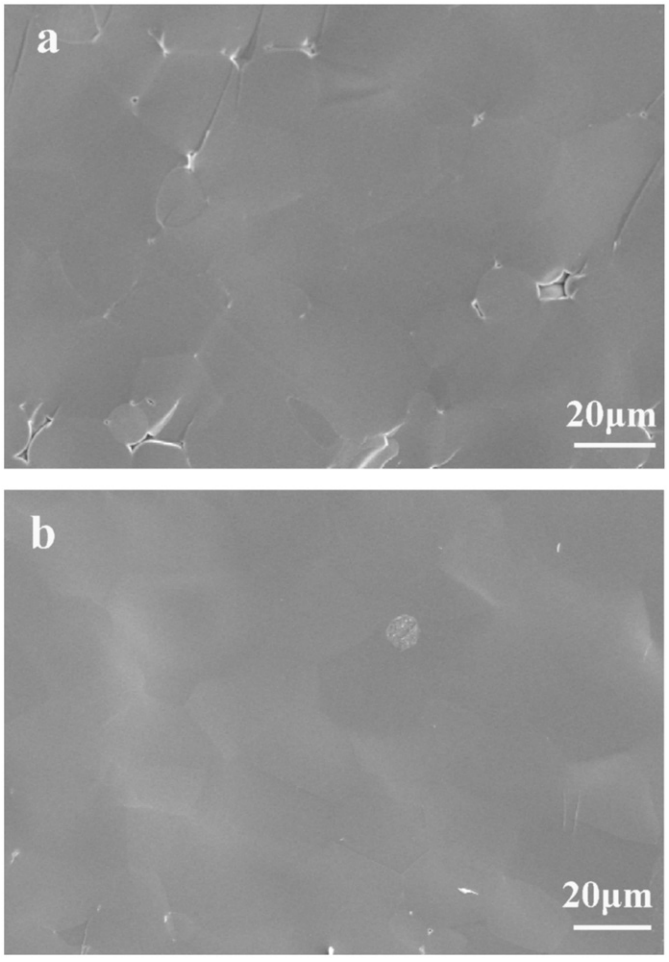

Fig. 4. SEM micrograph of the fracture surface of the bulk glasses hot-pressed at 905 °C (a) and 915 °C (b).

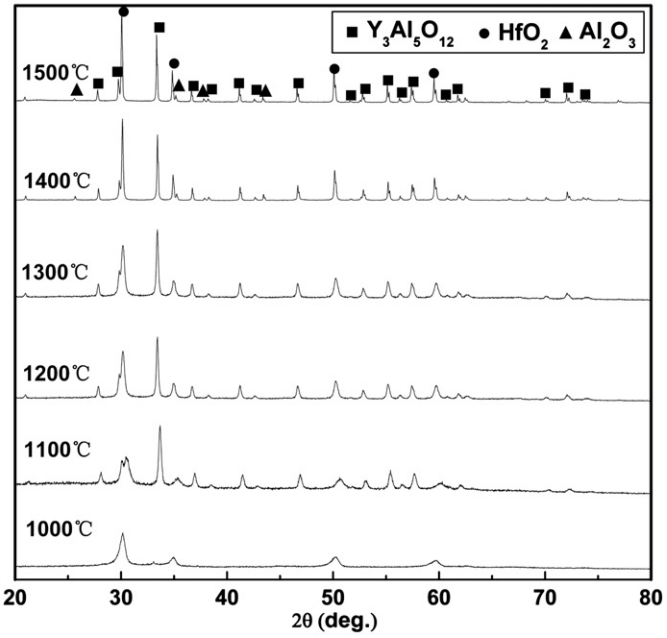

Fig. 5. XRD pattern of HAY ceramics annealed at different temperatures for 2 h.

annealing. In the present study, the crystallization starts from the HfO_2 phase having the lowest nucleation activation energy [7–9]. In addition, all of the three phases have good high-temperature stability, which is favorable to improve the mechanical properties of eutectic ceramics at high temperature.

TEM observation in Fig. 6(a) revealed that, the as-sintered bulk glass contained nano-crystallites of ~20–50 nm, which should be HfO_2 from XRD analysis (Fig. 3). After annealing at 1000 °C for 2 h, the HfO_2 crystallites grew up to 50–100 nm (Fig. 6(b)). Annealing at 1200 °C for 2 h brought the precipitation of YAG phase, the average size of which is below ~200 nm. However, more crystallization and grain growth, especially for YAG particles, occur after annealing at 1300 °C for 2 h, which cause the samples to lose their transparency (Fig. 7). After further annealing at 1400 or 1500 °C, the multi-phase ceramics with three identifiable phases, i.e. HfO_2, YAG and Al_2O_3 were obtained (Fig. 6(e) and (f)). Their transmittances in the infrared region are near zero because of the strong light scattering (Fig. 7).

Hardness and fracture toughness of the samples annealed at different temperatures were measured by the

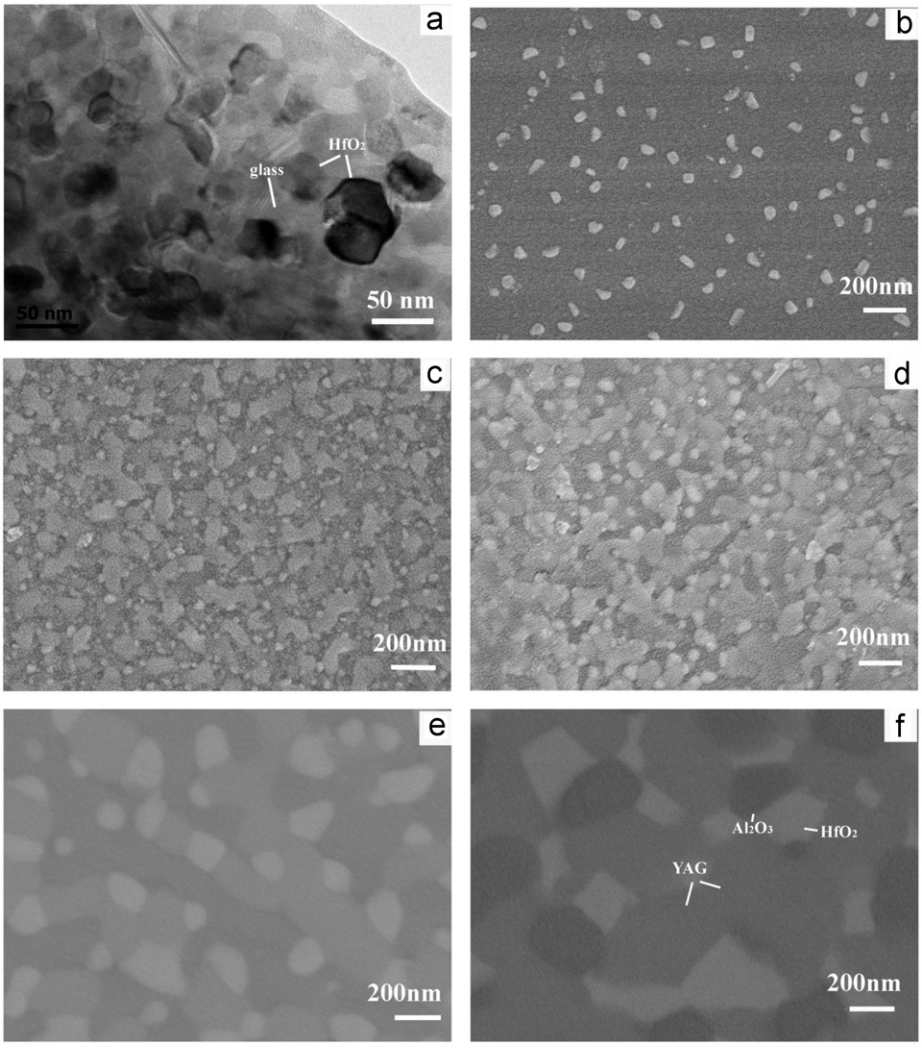

Fig. 6. SEM micrographs of the surface of HAY ceramics annealed at different temperatures: (a) glass hot-pressed at 915 °C, (b) 1000 °C, (c) 1200 °C, (d) 1300 °C, (e) 1400 °C and (f) 1500 °C.

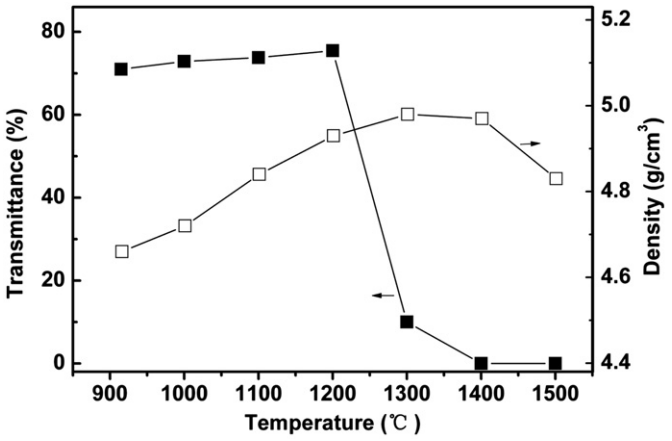

Fig. 7. Variations of transmittance and density as a function of the annealing temperature at the wavelength of 4.4 μm and the thickness of samples is 1 mm.

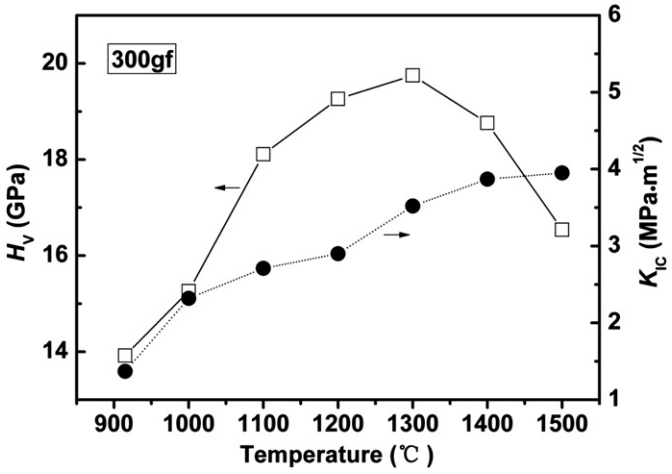

Fig. 8. Effects of annealing temperature on Vickers hardness (H_v) and fracture toughness (K_{IC}).

Vickers indentation method, as shown in Fig. 8. When the annealing temperature increases, the hardness of ceramics have the same change as their densities (Fig. 7), i.e. first increase and then decrease and the sample annealed at 1300 °C for 2 h has the maximum hardness of 19.8 GPa. Hardness of solidified ceramics is considered to be mainly dominated by the grain size of the Al_2O_3 phase, and the finer Al_2O_3 contributes to higher hardness [6,20,23]. At the initial annealing process, the hardness is limited by the presence of the much softer amorphous phase and do not fully benefit from their finer microstructure. However, the absence of glass-formers such as silica allows full crystallization at higher temperature. Therefore, the hardness of samples increases during the annealing process and has the top value after annealing at 1300 °C. However, further annealing at 1400–1500 °C results in grain growth, for example, the grain size of Al_2O_3 increases from several nanometers at 1200–1300 °C to over 200 nm at 1500 °C. Consequently, the hardness of samples annealed at higher temperature decreases.

The maximum hardness reported for directionally-solidified Al_2O_3–YSZ binary eutectics was 18–20 GPa and 13–16 GPa for Al_2O_3–YAG eutectics [6]. Su et al. produced the Al_2O_3–$Y_3Al_5O_{12}$–ZrO_2 ternary eutectic system by rapid solidification with a resulting hardness of 16.7 GPa [4]. In this work, a hardness of 19.8 GPa was observed for YAG/HfO_2/Al_2O_3 ternary eutectic ceramics, which is higher than Al_2O_3–$Y_3Al_5O_{12}$–ZrO_2 eutectics and comparable to Al_2O_3–ZrO_2 binary eutectics. From this result, the method reported here may be appropriate for preparing nano-crystalline eutectic ceramics with improved hardness.

During the annealing process, the fracture toughness keeps a linear increase ranging from 1.4 to 4.0 MPa m$^{1/2}$. This result agrees with the assertion of Peña et al. that higher fracture toughness for ternary ceramic can be found in a coarser microstructure because of stronger crack deflection and branching with the larger domain size [5].

4. Conclusions

Transparent glass-ceramics and hard eutectic ceramics in the HfO_2–Al_2O_3–Y_2O_3 system were prepared by amorphous sintering and post-annealing. By hot-pressing of glass microspheres from flame-quenching, transparent bulk glasses containing HfO_2 nano-crystallites were produced, showing a maximum transmittance of $>70\%$ in the infrared region. After annealing the bulk glasses at temperatures below 1200 °C, transparent glass-ceramics with HfO_2 crystallites of 100–200 nm were fabricated. By annealing at higher temperatures (>1300 °C), opaque YAG/HfO_2/Al_2O_3 eutectic ceramics were obtained. The maximum hardness of the eutectic ceramics reached 19.8 GPa, which is higher than that for the most ternary eutectic oxide ceramics prepared by rapid solidification, and such a higher hardness can be attributed to the presence of fine Al_2O_3 crystallites. The fracture toughness of the eutectic ceramics increased with increasing annealing temperature, and the maximum was 4.0 MPa m$^{1/2}$.

References

[1] J.M. Calderon-Moreno, M. Yoshimura, Nanocomposites from melt in the system Al_2O_3–YAG–ZrO_2, Scripta Materialia 44 (2001) 2153–2156.
[2] J.M. Calderon-Moreno, M. Yoshimura, Effect of melt quenching on the subsolidus equilibria in the ternary system Al_2O_3–$Y_3Al_5O_{12}$–ZrO_2, Solid State Ionics 141/142 (2001) 343–349.
[3] J.M. Calderon-Moreno, M. Yoshimura, Al_2O_3–$Y_3Al_5O_{12}$ (YAG)–ZrO_2 ternary composite rapidly solidified from the eutectic melt, Journal of the European Ceramic Society 25 (2005) 1365–1368.
[4] H. Su, J. Zhang, C. Cui, L. Liu, H. Fu, Rapid solidification of Al_2O_3/$Y_3Al_5O_{12}$/ZrO_2 eutectic in situ composites by laser zone remelting, Journal of Crystal Growth 307 (2007) 448–456.
[5] J.I. Peña, M. Larsson, R.I. Merino, I. de Francisco, V.M. Orera, J. LLorca, Processing, microstructure and mechanical properties of directionally-solidified Al_2O_3–$Y_3Al_5O_{12}$–ZrO_2 ternary eutectics, Journal of the European Ceramic Society 26 (2006) 3113–3121.
[6] J. LLorca, V.M. Orera, Directionally solidified eutectic ceramic oxides, Progress in Materials Science 51 (2006) 711–809.

[7] S. Araki, M. Yoshimura, Transparent nano-composites ceramics by annealing of amorphous phase in the HfO_2–Al_2O_3–$GdAlO_3$ system, International Journal of Applied Ceramic Technology 1 (2004) l55–l60.
[8] S. Araki, M. Yoshimura, Fabrication of transparent ceramics through melt solidification of near eutectic compositions in HfO_2–Al_2O_3–$GdAlO_3$ system, Journal of the European Ceramic Society 26 (2006) 3295–3299.
[9] A. Sugiyama, S. Araki, N. Sakamoto, Fabrication of amorphous bulk and multi-phase ceramics by melting method in the HfO_2–Al_2O_3–Gd_2O_3–Eu_2O_3 system, Journal of Electroceramics 17 (2006) 71–74.
[10] S.M. Lakiza, Ya.S. Tishchenko, V.P. Red'ko, L.M. Lopato, The Al_2O_3–HfO_2–Y_2O_3 phase diagram. I. Iosthermal sections at 1250 and 1650 °C, Powder Metallurgy and Metal Ceramics 48 (2009) 225–233.
[11] S.M. Lakiza, Ya.S. Tishchenko, A.O. Sus, Z.O. Zaitseva, L.M. Lopato, The Al_2O_3–HfO_2–Y_2O_3 phase diagram. II. Liquidus surface, Powder Metallurgy and Metal Ceramics 48 (2009) 693–699.
[12] S.M. Lakiza, Ya.S. Tishchenko, V.P. Red'ko, L.M. Lopato, The Al_2O_3–HfO_2–Y_2O_3 phase diagram. IV. Vertical sections, Powder Metallurgy and Metal Ceramics 49 (2010) 201–206.
[13] S.M. Lakiza, J.S. Tyschenko, L.M. Lopato, Phase diagram of the Al_2O_3–HfO_2–Y_2O_3 system, Journal of the European Ceramic Society 3 (2010) 1285–1291.
[14] L.L. Wang, L. Mei, G. He, G.H. Liu, J.T. Li, L.H. Xu, Z.J. Jiang, Preparation of Ce:YAG glass-ceramics with low SiO_2, Journal of the American Ceramic Society 11 (2011) 3800–3803.
[15] L. Mei, G. He, L.L. Wang, G.H. Liu, J.T. Li, Fabrication of transparent $LaAlO_3$/t-ZrO_2 nanoceramics through controlled amorphous crystallization, Journal of the European Ceramic Society 31 (2011) 1603–1609.
[16] L. Mei, G. He, L.L. Wang, G.H. Liu, J.T. Li, Controlled amorphous crystallization: an easy way to make transparent nanoceramics, Optical Materials 34 (2012) 981–985.
[17] L.L. Wang, L. Mei, G. He, G.H. Liu, J.T. Li, L.H. Xu, Z.J. Jiang, Preparation of infrared transparent YAG-based glass-ceramics with nano-sized crystallites, Journal of the European Ceramic Society (2012)http://dx.doi.org/10.1016/j.jeurceramsoc.2012.03.023.
[18] G. He, L. Mei, L.L. Wang, G.H. Liu, J.T. Li, Synthesis and luminescence properties of nano-/microstructured $Y_3Al_5O_{12}$:Ce^{3+} microspheres by controlled glass crystallization, Crystal Growth and Design 11 (2011) 5355–5361.
[19] A. Prnová, R. Karell, D. Galusek, The preparation of binary Al_2O_3–Y_2O_3 glass microspheres by flame synthesis from powder oxide precursors, Ceramics – Silikaty 52 (2008) 109–114.
[20] A. Rosenflanz, M. Frey, B. Endres, Bulk glasses and ultrahard nanoceramics based on alumina and rare-earth oxides, Nature 430 (2004) 761–764.
[21] S. Inaba, S. Fujino, Empirical equation for calculating the density of oxide glass, Journal of the American Ceramic Society 93 (2010) 217–220.
[22] K. Niihara, A fracture mechanics analysis of indentation-induced Palmqvist crack in ceramic, Journal of Materials Science Letters 2 (1983) 221–223.
[23] A. Larrea, V.M. Orera, R.I. Merino, J.I. Peña, Microstructure and mechanical properties of Al_2O_3–YSZ and Al_2O_3–YAG directionally solidified eutectic plates, Journal of the European Ceramic Society 25 (2005) 1419–1429.